Modeling of the Modulation by Buffers of Ca^{2+} Release through Clusters of IP_3 Receptors

S. Zeller,[†] S. Rüdiger,[‡] H. Engel,[†] J. Sneyd,[§] G. Warnecke,[¶] I. Parker,[‖] and M. Falcke[††*]

[†]Institute for Theoretical Physics, Technische Universität Berlin, Berlin, Germany; [‡]Institute of Physics, Humboldt-University of Berlin, Berlin, Germany; [§]Department of Mathematics, University of Auckland, Auckland, New Zealand; [¶]Institute for Analysis and Numerical Mathematics, Otto-von-Guericke University Magdeburg, Magdeburg, Germany; [‖]Department of Neurobiology and Behavior, University of California, Irvine, California; and [††]Mathematical Cell Physiology, Max Delbrück Centre for Molecular Medicine, Berlin, Germany, and Department of Theoretical Physics, Helmholtz Zentrum Berlin, Berlin, Germany

ABSTRACT Intracellular Ca^{2+} release is a versatile second messenger system. It is modeled here by reaction-diffusion equations for the free Ca^{2+} and Ca^{2+} buffers, with spatially discrete clusters of stochastic IP_3 receptor channels (IP_3Rs) controlling the release of Ca^{2+} from the endoplasmic reticulum. IP_3Rs are activated by a small rise of the cytosolic Ca^{2+} concentration and inhibited by large concentrations. Buffering of cytosolic Ca^{2+} shapes global Ca^{2+} transients. Here we use a model to investigate the effect of buffers with slow and fast reaction rates on single release spikes. We find that, depending on their diffusion coefficient, fast buffers can either decouple clusters or delay inhibition. Slow buffers have little effect on Ca^{2+} release, but affect the time course of the signals from the fluorescent Ca^{2+} indicator mainly by competing for Ca^{2+}. At low [IP_3], fast buffers suppress fluorescence signals, slow buffers increase the contrast between bulk signals and signals at open clusters, and large concentrations of buffers, either fast or slow, decouple clusters.

INTRODUCTION

Cellular functions such as gene expression, secretion, muscle contraction, and synaptic plasticity depend on intracellular Ca^{2+} signaling. Changes of the cytosolic Ca^{2+} concentration are organized into spatio-temporal patterns like localized transients (1), propagating waves (2–4), and global oscillations (5,6).

In many cells, these changes in free cytosolic Ca^{2+} concentration result from the release of Ca^{2+} from the endoplasmic reticulum (ER). Release occurs via intracellular Ca^{2+} channels, notably inositol 1,4,5-trisphosphate receptors (IP_3R), and Ca^{2+} is then resequestered into the ER by Ca^{2+} pumps (SR/ER Ca^{2+}-ATPases). IP_3Rs are regulated by the Ca^{2+} they conduct; the stationary open probability of the IP_3Rs is a bell-shaped function of Ca^{2+} concentration, so that a small rise increases the open probability, whereas a larger increase in Ca^{2+} concentration decreases the open probability. In addition, the time course of the Ca^{2+} concentration is important; a step increase leads to an initial activation of the IP_3Rs, followed by a slower inhibition (7,8).

Within the membrane of the ER, clusters of IP_3Rs are separated by perhaps 1–7 μm (3,9,10). These clusters of channels generate global concentration spikes via a hierarchy of Ca^{2+} release events (1,11) that depend upon Ca^{2+} diffusing between IP_3Rs to ignite the activity of successive clusters (4,12). The smallest Ca^{2+} release events, i.e., blips (1), probably reflect random openings of single IP_3Rs. Larger events, i.e., puffs, lasting tens of milliseconds and restricted to a volume of <0.5 fL, reflect the almost simultaneous opening of several IP_3Rs within a cluster (1,3,9,10). Many coordinated puffs form oscillations and waves (4,13). Ca^{2+} oscillations therefore depend upon both the spatial organization of IP_3Rs and their regulation by Ca^{2+} (8,14,15).

Cytosolic concentration transients are modulated by the buffering of free Ca^{2+} ions by various cytosolic Ca^{2+} binding proteins (16,17) or exogenous buffers (18). Moreover, the fluorescent indicator dyes used to image intracellular Ca^{2+} represent an additional, exogenous Ca^{2+} buffer. Since buffers bind free Ca^{2+}, they change the effective transport of Ca^{2+} between release sites. Some buffers, such as bis-ethane-*n*,*n*,*n*′,*n*′-tetraacetic acid (BAPTA), have fast on- and off-rates for Ca^{2+}, whereas other buffers, such as ethylene glycol tetraacetic acid (EGTA), have much slower Ca^{2+} binding kinetics. It has long been known that fast buffers not only change effective diffusion, but also slow down the timescale of Ca^{2+} concentration changes by a factor

$$\left[1 + \sum_i B_i K_i/(K_i + c)^2\right]^{-1}$$

(4,19), where B_i is the total concentration of the buffer, and K_i is its dissociation constant. The index i denotes the different buffer species, and c denotes the free Ca^{2+} concentration.

The positive feedback by Ca^{2+} provides a self-amplifying release mechanism called calcium-induced Ca^{2+} release. Ca^{2+} released by an open cluster diffuses through the cytosol and increases the open probability of neighboring clusters. It thereby synchronizes Ca^{2+} release over a wide area, thus generating complex spatio-temporal signals.

Submitted October 21, 2008, and accepted for publication May 12, 2009.

*Correspondence: martin.falcke@mdc-berlin.de

Editor: Herbert Levine.

0006-3495/09/08/0992/11 $2.00

doi: 10.1016/j.bpj.2009.05.050

Channels within a cluster are strongly coupled due to the tight packing and large local concentrations (20). Local concentrations are large, since even small currents going through pores of molecular dimensions cause large flux densities (20). Clusters in turn are distributed across the ER membrane at spacings of a few micrometers. The coupling between clusters is much weaker than between the channels within a cluster.

As a consequence of the existence of a hierarchy of length scales and coupling strengths, the dynamics of the cell are not identical with the local dynamics, but depend on the properties of spatial coupling within the cell. That coupling is the diffusion of Ca^{2+} and can be modified by buffers (21). Buffers with concentrations of a few tens of μM mainly change the way IP_3Rs interact, with little effect on the properties of individual IP_3Rs, since they cannot compete with the large local flux density at open channels (20,22). Hence, they are the ideal tool to investigate the spectrum of emergent behaviors that arise from the interactions of many IP_3Rs. In repetitively spiking systems, global spikes become first less probable and then disappear with increasing buffer concentrations (21,23,24). This effect results from low buffer concentrations that have negligible effect on Ca^{2+} diffusion within a cluster (20,22), suggesting that buffers act on the length scale of cluster spacing but not within clusters at small concentrations.

Whereas our previous studies focused on repetitively spiking cells (24,25), here we study the effects of high buffer concentrations on the initial spike after onset of stimulation. We relate our results to analogous experimental studies by Dargan et al. (17) and Dargan and Parker (18), who found that the response of the Ca^{2+} signal to exogenous buffer depends on the binding kinetics of Ca^{2+} to the buffer. In these experiments, buffer was initially injected or loaded into the cell, the IP_3 concentration was increased in stepwise fashion, and the amount of Ca^{2+} in the cytosol was measured by fluorescence recordings using an additional dye buffer. It was found that large concentrations of EGTA (a slow buffer) shape the fluorescence signal, whereas large concentrations of BAPTA (a fast buffer) shape the time course of Ca^{2+} release. The slow Ca^{2+} chelator parvalbumin was found to produce results very similar to EGTA, and the fast chelator calretinin had effects very similar to BAPTA (17). Interestingly, BAPTA and EGTA have similar Ca^{2+} affinities.

The article is organized as follows: first, we introduce the basic Ca^{2+} dynamics model, including a stochastic model of channel state transitions, and briefly discuss the adaptive scheme used to solve the deterministic and stochastic equations. We then present results of simulations, first for a small amount of endogenous buffer, then, for varying amounts of fast and slow exogenous buffer. Parameters were chosen to match BAPTA and EGTA. The last section summarizes our findings and relates them to other experiments dealing with the impact of buffers on Ca^{2+} signals.

PARTIAL DIFFERENTIAL EQUATIONS FOR CONCENTRATIONS AND STOCHASTIC MODEL OF CHANNEL GATING

IP_3Rs consist of four identical subunits. The stochastic evolution of the state of each subunit is determined by a continuous-time Markov chain, which is described by a state scheme and transition rates according to the DeYoung-Keizer model (23,26) (see Fig. S2 in the Supporting Material). Some of the transition rates depend on the local Ca^{2+} or IP_3 concentration. The Ca^{2+} concentration is calculated, as a function of space and time, in a thin two-dimensional sheet close to the plasma membrane. IP_3R clusters are positioned at discrete places in the ER membrane (see $P_{ch}(\vec{r},t)$ in Eq. 1 below). When a channel is open, a Ca^{2+} current appears as a source term in the reaction-diffusion equation for the Ca^{2+} concentration.

Channel state dynamics and concentration dynamics are coupled. Random opening and closing of the channels causes changes in the source terms in the partial differential equations, whereas, conversely, the transition rates of the Markov model of each subunit depend on the local Ca^{2+} concentration.

Details of the mathematical model are explained in the Supporting Material. The cytosolic Ca^{2+} concentration, c, is controlled by diffusion, transport of Ca^{2+} through the ER membrane, and reaction with Ca^{2+} buffers. We consider three types of buffers: an exogenous mobile buffer b_m with either slow or fast reaction kinetics, a stationary buffer b_s with fast kinetics, and an exogenous dye buffer b_d. Total concentrations of buffers are denoted by B_m, B_s, and B_d. The partial differential equations read:

$$\begin{aligned}\frac{\partial c}{\partial t} &= D\nabla^2 c + (P_l + P_{ch}(\vec{r},t))(ER_{const} - c) - P_p\frac{c^2}{K_d^2 + c^2} \\ &\quad + k_c(c_0 - c) - k_s^+(B_s - b_s)c + k_s^- b_s \\ &\quad - k_m^+(B_m - b_m)c + k_m^- b_m - k_d^+(B_d - b_d)c + k_d^- b_d, \end{aligned} \tag{1}$$

$$\frac{\partial b_s}{\partial t} = k_s^+(B_s - b_s)c - k_s^- b_s, \tag{2}$$

$$\frac{\partial b_m}{\partial t} = D_m\nabla^2 b_m + k_m^+(B_m - b_m)c - k_m^- b_m, \tag{3}$$

$$\frac{\partial b_d}{\partial t} = D_d\nabla^2 b_d + k_d^+(B_d - b_d)c - k_d^- b_d. \tag{4}$$

Here, the $k_l^{\pm}$ (l = s, m, d) denote the on- and off-rates of Ca^{2+} reacting with the corresponding buffers. A complete list of the buffer parameters is given in Table S1. The equations are solved in a domain of (33 μm)^2 (in some cases of (49.5 μm)^2).

Ca^{2+} moves from the ER to the cytosol through IP_3 receptor channels and by a small leak flux (terms with coefficients P_{ch} and P_l, respectively), and Ca^{2+} is resequestered

into the ER by pumps (P_p). The action of pumps is assumed to be cooperative and modeled by a second-order Hill function with dissociation constant K_d. The receptor term P_{ch} in Eq. 1 models the current through the channel. It vanishes if all channels in a cluster are closed. The term $k_c(c_0 - c)$ in the equation for c describes the transport of Ca^{2+} through the plasma membrane. It forces the resting concentration of free Ca^{2+} to be equal to c_0.

In our simulations we have placed 5×5 clusters, with 10 channels each, on a quadratic lattice, with each cluster separated by a distance of $d = 3$ μm (see Fig. S1). When the grid size is $(49.5\ \mu m)^2$, d is chosen to be 4.5 μm.

RESPONSES AFFECTED BY EXOGENOUS BUFFER WITH LARGE DIFFUSION COEFFICIENT

The results of control simulations without an exogenous buffer are explained in Fig. S3. They demonstrate that release typically starts with a peak in the number of open channels with a full duration at half-maximum of ~150 ms (initial spike), followed by a phase with much smaller numbers of open channels (release tail). The average full duration at half-maximum of the control fluorescence signal increases from 3.3 s to 3.9 s when we increase $[IP_3]$ from 0.09 μM to 0.62 μM. This is in qualitative agreement with experiments, but is less than measured increases. Fig. 1 shows the line-scan plots for typical runs with an exogenous buffer. Due to the stochastic nature of the onset of release, the time delay for the opening of the first channel varies between the panels of Fig. 1. The average delay from the IP_3 step until the opening of the first channel is independent of the type of buffer applied and the buffer concentration, since the resting Ca^{2+} concentration is independent of the buffer. Therefore, we can shift the zero time of each run and align the moments of different runs when the spatially averaged Ca^{2+}-bound dye crosses the 15 μM level. That was chosen as a mark for the onset of global release. This practice will be used when we calculate averages over several runs in our analysis below.

At low $[IP_3]$, BAPTA strongly suppresses fluorescence signals. Since it does not change the resting concentration of free Ca^{2+}, it does not abolish spontaneous channel openings. However, BAPTA reduces activation of further channels and thus the number of measurable events. Events shorter than 20 ms (the scan interval) still occur. EGTA separates individual release events with respect to the fluorescence signal. As we will discuss below in detail, EGTA steepens temporal gradients of fluorescent Ca^{2+}-bound dye. It therefore also steepens spatial gradients, rendering individual events more readily distinguishable than in the absence of EGTA. EGTA also reduces mutual activation between clusters. Approximately 70% of control runs show global release events in the first 10 s after the IP_3 step increase, whereas only ~30% do with 200 μM EGTA. The number of isolated puffs is similar in control and EGTA simulations. Both the results with BAPTA and EGTA at low $[IP_3]$ agree well with experiments (17,18).

The initial spike of Ca^{2+}-bound dye, b_d, in Fig. 1 *b* is much shorter with large EGTA concentrations than in the control case. This shortened duration is related to the slow kinetics of the buffer (see below). This effect can also be seen in Fig. 2 *a*, where we show b_d for several EGTA concentrations.

We also observe in Fig. 1 *b* that, in the presence of BAPTA, the concentration of b_d decays much slower, or not at all, within the time interval shown. The fast buffer causes the concentration of Ca^{2+}-bound dye to become almost homogeneous soon after the onset of release. Additionally, values of b_d are substantially larger in the release tail than with EGTA or in the control (see also Fig. 2). All of these observations agree well with the experimental results in Dargan and Parker (18).

Fig. 2 summarizes results for the spatial average of Ca^{2+}-bound dye, b_d, for many simulations. We averaged along the scan line used in Fig. 1. The control case shows a pronounced maximum corresponding to the spike in the number of open channels. We observe a decrease of that maximum with rising buffer concentration. BAPTA reduces it more effectively than EGTA. When the concentration of BAPTA is large, the time course of b_d is a monotonic increasing function of time, and approaches an asymptotic value.

The slow buffer EGTA shapes the time course of Ca^{2+}-bound dye concentration

The spike b_d exhibits a pronounced maximum in the presence of EGTA, and the decay of Ca^{2+}-bound dye after the maximum is even faster with EGTA than in the control. There are two possible explanations for the acceleration of the decay by EGTA. First, it might arise as a result of the transfer of Ca^{2+} away from the scan line to the cluster-free areas by diffusing Ca^{2+}-bound EGTA molecules. We call this effect ''shuttling''. The binding to EGTA, which diffuses, keeps Ca^{2+} ions from being caught by stationary buffer, which does not diffuse. Thus, EGTA can increase the total Ca^{2+} diffusion.

Alternatively, the decay may be accelerated by competition between the dye and EGTA. The dye competes with the other buffers for free Ca^{2+}. How much Ca^{2+} is taken up by a particular buffer, and how quickly this happens, depends on the kinetic parameters of all the buffers. The initial response will depend on the ratios of the on-rates of the buffers. The dye is fast and reaches the (quasi-)stationary value of its Ca^{2+}-bound fraction quickly. EGTA is slow and keeps binding Ca^{2+} after the dye has reached its quasistationary value. It thereby decreases the concentration of free Ca^{2+} which, in turn, causes Ca^{2+} to dissociate from the dye. This redistribution of Ca^{2+} from the dye to EGTA contributes to the decay of fluorescence. We will investigate below to which degree both mechanisms—shuttling and competition—contribute to the fast decay of the dye signal with large EGTA concentration.

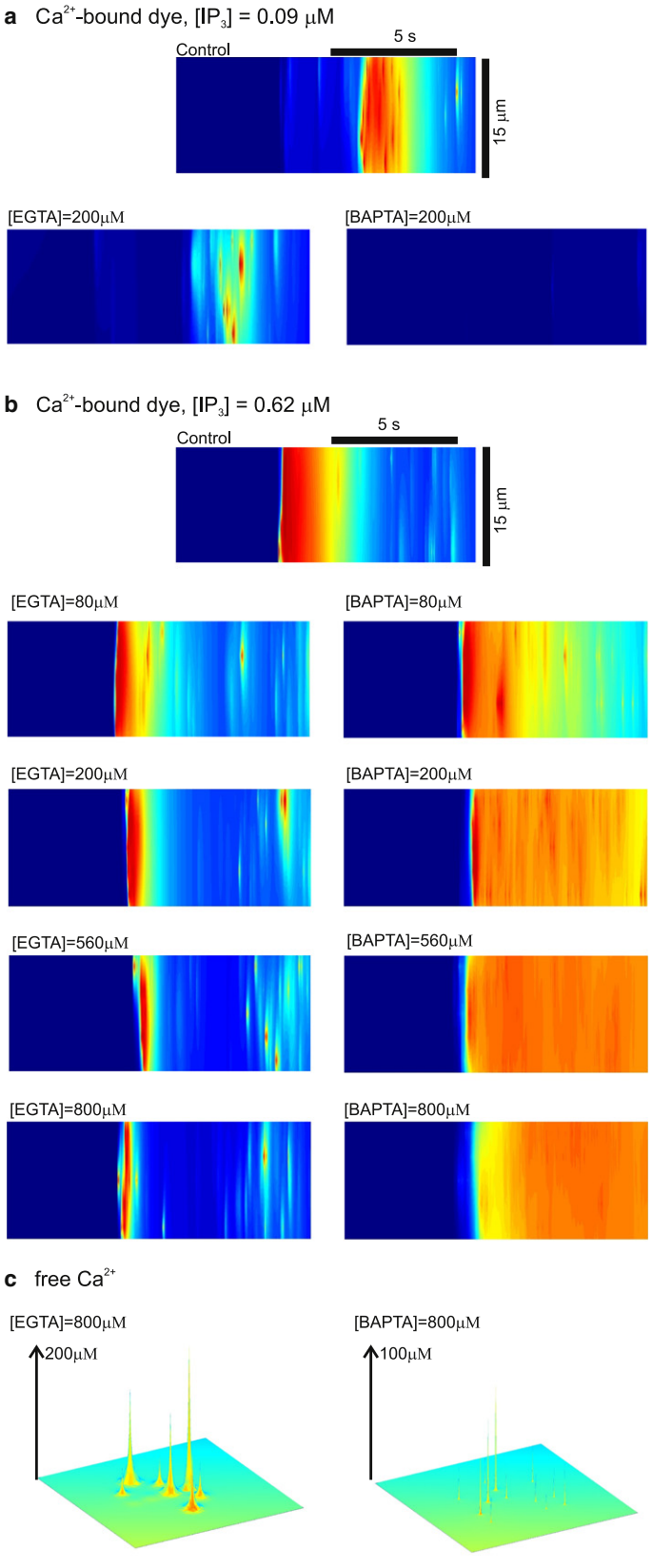

FIGURE 1 (*a*) Space-time plot of Ca^{2+}-bound dye concentrations b_d for $[IP_3] = 0.09\ \mu M$ scanned across the cluster area (see also Fig. S1). Shown are control results and simulations with 200 μM BAPTA and EGTA. (*b*) Space-time plot of Ca^{2+}-bound dye concentrations b_d for $[IP_3] = 0.62\ \mu M$ and different concentrations of EGTA and BAPTA scanned across the cluster area. (*a* and *b*) Blue indicates low concentrations; red values are those close to B_d (see Table S2). (*c*) Snapshots of the concentration of free Ca^{2+} during a release spike. The needles mark the location of clusters with open channels; they show the concentration of free Ca^{2+} in a puff. In a range of a few tens of nanometers around an open cluster, they form within microseconds upon channel opening and collapse comparably fast. The long-range spatial modes of the concentration profiles remaining after the collapse have amplitudes of a few μM only and decay with timescales of a few hundred milliseconds (20). Puffs last typically a few tens of milliseconds.

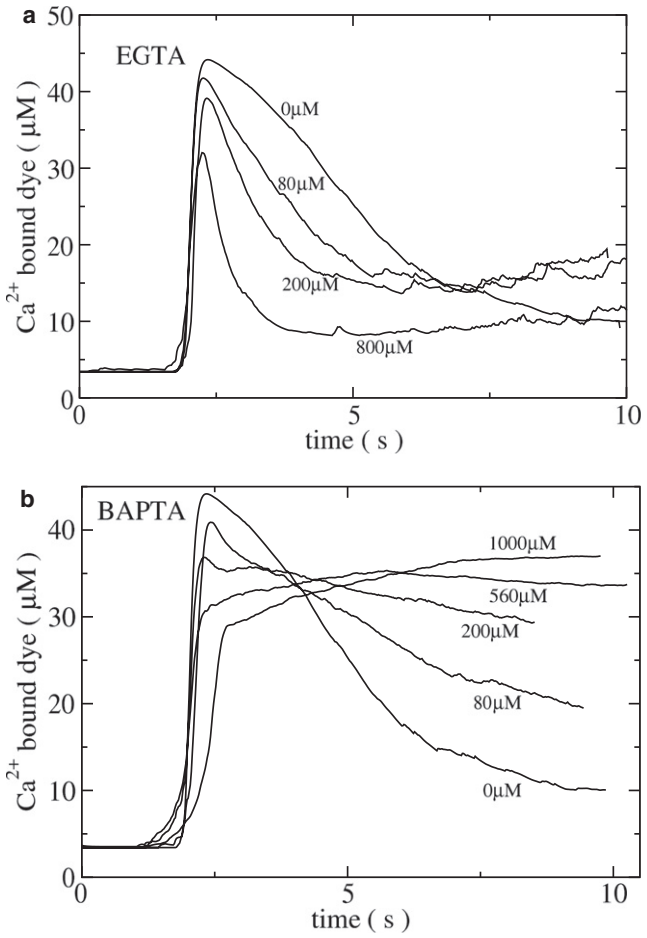

FIGURE 2 Evolution of the concentration of Ca^{2+}-bound dye averaged along a line in the middle of the cluster field (see Fig. S1). The curves are ensemble averages for 10 runs.

We use a dissociation constant $K_d^m = 0.12\ \mu M$ for EGTA, which is approximately one-half of the value for BAPTA and the dye buffer. The acceleration of fluorescence decay occurs also for equal values of the dissociation constants of mobile exogenous buffer (K_d^m) and dye (K_d^d), as demonstrated in Fig. S5. It also works with a variety of rate values for EGTA. Hence, the difference between the behavior with high EGTA concentrations and high BAPTA concentrations can be explained simply by the different rate constants of the buffers. We base that conclusion also on an earlier simulation study showing a transition from spiking behavior to maintained release simply by increasing the value of the buffer rate constants (see (21), their Fig. 9).

The comparison between control conditions ([EGTA] = [BAPTA] = 0 μM) and [EGTA] = 560 μM in Fig. 3 *a* shows the substantial contribution of EGTA to the decay of b_d. The different contributions of the shuttle effect and of buffer competition can be dissected by comparing the time course of the line-scan average with the bulk average, and by varying the buffer diffusion coefficients. Fig. 3 *a* shows bulk averages across the whole integration field and line averages. The bulk average is not influenced by the shuttle effect since it takes into account changes of b_d in the outer cluster-free region (see Fig. S1) to which Ca^{2+} may have been shuttled. We find that the line average with [EGTA] = 560 μM decays only slightly faster than the bulk average, i.e., diffusion contributes little to the decay of the line average. Both time constants are approximately twice the time constants of the slow long-range spatial modes of the concentration profile found in detailed three-dimensional simulations without large EGTA concentrations (20). Hence, very early during the decay, the profile gradient is flat, and therefore cannot drive large diffusion fluxes.

Note that the outer cluster free region has an area of 945 μm^2, much larger than the area of the cluster region which is only 144 μm^2, and can therefore accommodate a large amount of a diffusing species. Furthermore, the value $k_m^- = 0.06\ s^{-1}$ of the rate for Ca^{2+}-dissociation from EGTA is sufficiently small to allow shuttling of Ca^{2+} ions by diffusing EGTA molecules from the center of the cluster field to the outer region. Hence, lack of space or the value of the dissociation constant of the diffusing species are unlikely to limit the shuttle effect.

Fig. 3 *b* shows the time course of Ca^{2+}-bound EGTA, b_m. It rises quickly upon onset of release, saturates and does not decay for seconds afterwards. Its decay is so slow because its behavior after the quick rise approximately follows that of total cytosolic Ca^{2+} ($c + b_d + b_m + b_s$) (data not shown). The timescale of total cytosolic Ca^{2+} is slow because it is proportional to the inverse of the total buffer capacity. It is therefore slow even with a rather small [EGTA] of 80 μM (4,19). Over the time range where b_d decays, the time course of Ca^{2+}-bound EGTA can be fit to exponential functions. The time constants of the decay of the line average of b_d approach those for the rise of the bulk average of Ca^{2+}-bound EGTA for large EGTA concentrations (see Fig. 3 *c*). These findings show that buffer competition between the fast and slow buffers determines the decrease of the fluorescence signal, when the EGTA concentration is large. In line with that, changing the buffer diffusion coefficients from 200 $\mu m^2\ s^{-1}$ to 20 $\mu m^2\ s^{-1}$ has little effect on the time constant of dye decay (Fig. 3 *c*). However, increasing the EGTA on-rate from $k_m^+ = 0.5\ (\mu M\ s)^{-1}$ to $k_m^+ = 2.0\ (\mu M\ s)^{-1}$, while keeping K_d^m constant, reduces τ_d from 0.61 s to 0.30 s (see Fig. 3 *d*). Indeed, the rate of b_d decay, τ_d^{-1}, is approximately a linear function of k_m^+.

BAPTA, however, has a faster on-rate than EGTA. Therefore, binding of Ca^{2+} will occur simultaneously with both buffers, dye and BAPTA, and delayed redistribution of Ca^{2+} to BAPTA does not occur. Hence, the stronger decay of Ca^{2+}-bound dye, which is observed with EGTA, is not observed in the case of BAPTA.

BAPTA shapes the time course of release by delaying Ca^{2+}-dependent inhibition

Not only does BAPTA shape the time course of Ca^{2+}-bound dye, it also shapes the time course of Ca^{2+} release. Fig. 4 shows the evolution of the number of open channels for

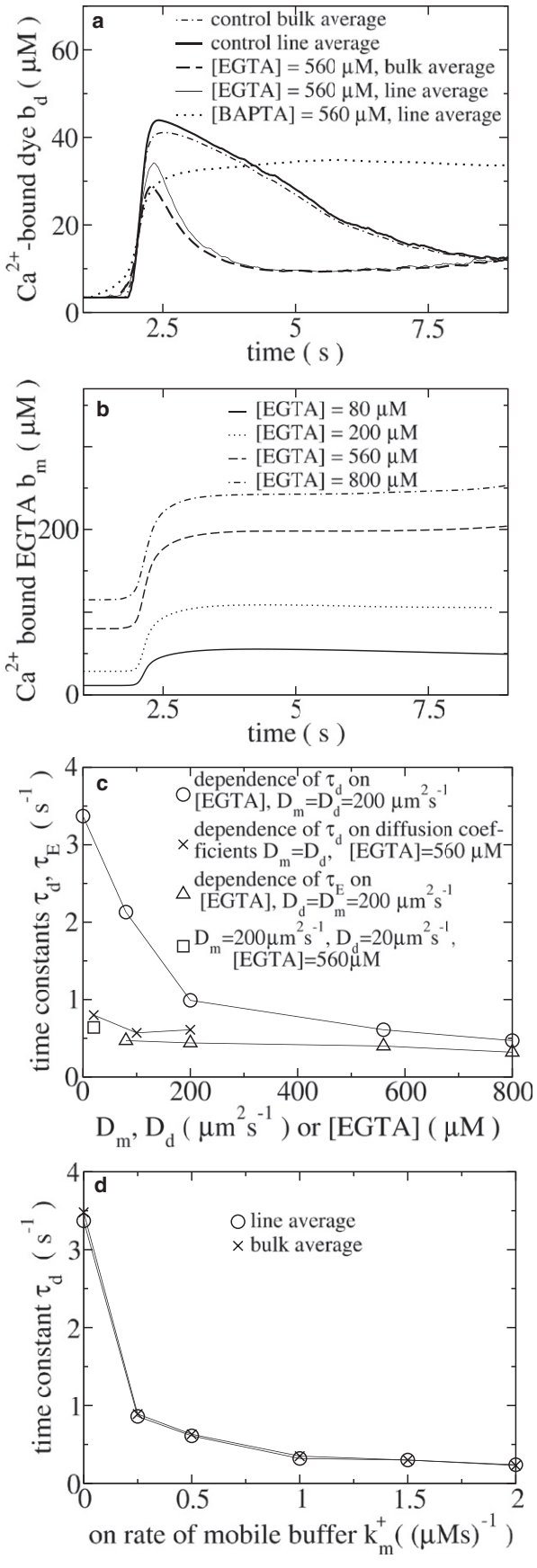

different EGTA and BAPTA concentrations. Compared to the control, BAPTA spreads out release in time; at higher BAPTA concentrations, the number of open channels increases more slowly and decays more slowly.

When [BAPTA] = 80 μM, the peak number of open channels is smaller than the control value, but the peak increases with increasing concentration for [BAPTA] $\geq$ 200 μM. In particular, the number of open channels after the spike is larger with large BAPTA concentrations than with large EGTA concentrations or control conditions.

That can be explained by delayed Ca^{2+}-dependent inhibition as the time course of the number of inhibited channels tells us (Fig. 5). A control spike in the number of open channels lasts ~0.3 s. The number of inhibited channels at about that time after onset of release is significantly smaller with large BAPTA concentrations than with large EGTA concentrations or the control values. In particular, the fraction of channels which can open is substantially larger with large [BAPTA] than with large [EGTA]. It increases from ~0.06 to 0.18 when we replace 800 μM EGTA by 800 μM BAPTA. In addition, once a channel has opened, the release of Ca^{2+} favors opening of more channels. This explains the larger number of open channels in the release tail with BAPTA compared to corresponding EGTA applications.

Local concentrations at open clusters determine the rate of Ca^{2+}-dependent inhibition

Inhibition is slowed down with large BAPTA concentrations since BAPTA reduces the local concentration at open clusters from typical values of 120 μM in the control, to typical values of 40 μM with [BAPTA] = 800 μM. The rise of free Ca^{2+} at closed clusters resulting from adjacent open clusters does not contribute substantially to Ca^{2+}-dependent inhibition. That argument is substantiated by the data in Fig. S4. The addition of 800 μM EGTA reduces the bulk average by a factor of ~1/15 (see Fig. S4 *a*). If inhibition would be dominated by bulk concentrations, it should go down

FIGURE 3 (*a*) Representative time courses of the bulk average and line average of b_d. The curves are ensemble averages over 10 runs each. The time courses of the control simulations and EGTA-simulations exhibit decay after their maxima, which can be fit to exponential functions $A_0 \exp(-t/\tau_d) + A_1$. The control simulations decay with a time constant of 3.37 s (*line*) and 3.48 s (*bulk*); the line average with 560 μM EGTA decays with a time constant of 0.61 s and the bulk average with 0.63 s. (*b*) Ca^{2+}-bound EGTA (b_m) in dependence upon time for different EGTA concentrations. The time courses of b_m from about the point of steepest slope to time $\approx$4.5 s can be fit to exponential functions $A_2 \exp(-t/\tau_E) + A_3$. (*c*) Only the τ_d of the line average in dependence upon the buffer diffusion coefficients D_d and D_m and the EGTA concentration, and τ_E in dependence on the EGTA concentration, are shown here. The abscissa shows the value of the diffusion coefficients D_d and D_m (with $D_d = D_m$) for the $\times$ symbols and the EGTA concentration for the $\bigcirc$ and $\triangle$ symbols. The $\square$ symbol shows τ_d for $D_d = 20$ μm^2 s^{-1} and $D_m = 200$ μm^2 s^{-1}. Fast diffusion of EGTA does not speed up the decay compared to the case with dye and EGTA diffusing slowly. (*d*) τ_d in dependence on k_m^+ with [EGTA] = 560 μM, $D_d = D_m = 200$ μm^2 s^{-1}, and $K_d^m = 0.12$ μM.

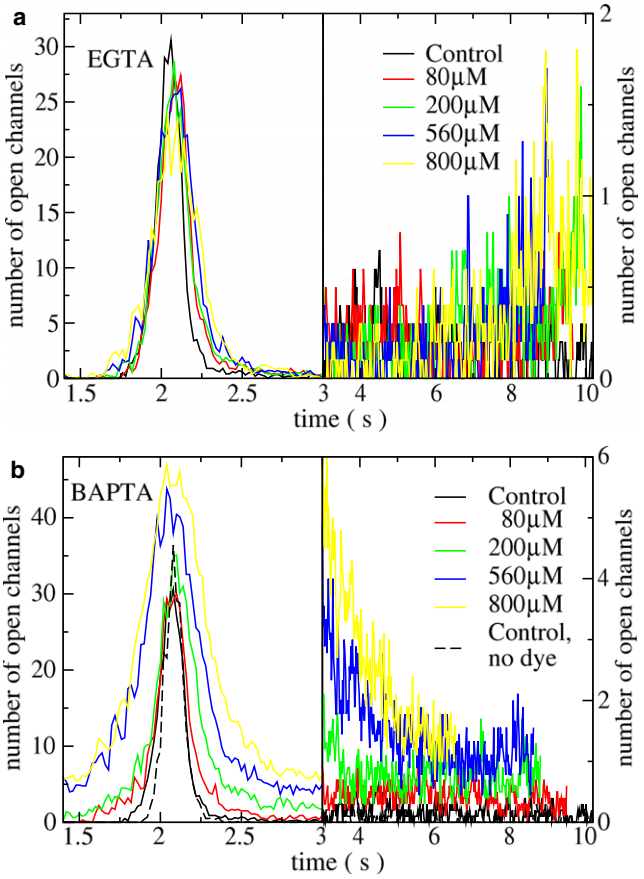

FIGURE 4 Evolution of the number of open channels averaged over 10 runs for each amount of EGTA and BAPTA concentration. We change the scaling of the y axis at $t = 3$ s to meaningfully resolve the number of open channels in the tail region. The BAPTA-panel also shows the number of open channels without any exogenous buffer (control, no dye). The maximum number is larger and the peak even shorter than in the control case with dye. The number of open channels in the tail region is smaller than control.

comparably. Instead, the much smaller reduction of Ca^{2+} peak values in Fig. S4 *b* by the same amount of EGTA is in line with the results about inhibition. The stronger effect of BAPTA on peak values corresponds to the decreased inhibition observed with that buffer.

These findings explain why even the large EGTA concentrations do not delay inhibition. The local dynamics of free Ca^{2+} at open clusters are dominated by the channel flux with a value of ~10^6 μM s^{-1} and diffusion fluxes of the same order of magnitude. Because of the small rate constants, the EGTA reaction terms are approximately two orders-of-magnitude smaller, even with concentrations of 800 μM. The BAPTA reaction terms are of the same order of magnitude as the channel flux.

The interactions between local concentration and inhibition have important consequences for modeling, as models based on spatially averaged concentrations do not capture the large local fluxes, or large local concentrations, at open channels. Such averaged models would provide a time

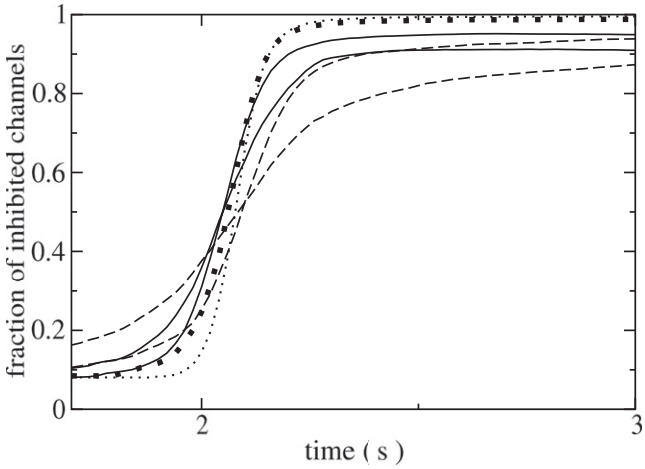

FIGURE 5 Evolution of the fraction of inhibited channels averaged over 10 runs for each EGTA and BAPTA concentration. The thick dotted line shows control, the thin dotted line is control without dye. The solid lines show simulations with EGTA as exogenous buffer and the dashed lines with BAPTA. The [EGTA] and [BAPTA] values are 200 μM and 800 μM from larger to smaller values of the fraction of inhibited channels at late time.

course of free Ca^{2+} like the bulk average in Fig. S4, thus giving qualitatively different results from a model which treats the local concentrations more accurately.

The effect of an exogenous buffer with a small diffusion coefficient

There is a large variety of reported values of the diffusion coefficient of EGTA, BAPTA, or FURA2 in the cytosol (BAPTA and EGTA: 183 $\mu m^2\ s^{-1}$ (27), 171 $\mu m^2\ s^{-1}$ (28), and 39 $\mu m^2\ s^{-1}$ (29)). Modelers use values between 20 and 250 $\mu m^2\ s^{-1}$ (4). The value of 200 $\mu m^2\ s^{-1}$ was taken from Dargan and Parker (18) and is used also in Klingauf and Neher (30). However, the diffusion coefficient may be smaller, as in striated muscle cells (39 $\mu m^2\ s^{-1}$ (29)), and the diffusion coefficients of the Ca^{2+} chelators parvalbumin and calretinin were found to be ~40 $\mu m^2\ s^{-1}$ (17,31), or even as low as 12 $\mu m^2\ s^{-1}$ (32). Therefore we simulated the effects of buffers with small diffusion coefficients, $D_m = D_b = 20\ \mu m^2\ s^{-1}$.

We observe also a transition to a monotonic increase of b_d with increasing BAPTA concentrations, larger values of b_d with BAPTA than with EGTA in the tail region, and a decay of b_d with large concentrations of EGTA, which is faster than control. Again, increasing the EGTA or BAPTA concentrations reduces the maximum of b_d. These results with small buffer diffusion are similar to those with large buffer diffusion.

However, substantial differences between simulations with large and small buffer diffusion coefficients appear in the time course of the number of open channels. When [BAPTA] is large, the relatively slow rise time of the dye signal (Fig. 6) indicates that the number of open channels rises slowly. Fig. S6 confirms that. Indeed, the main difference between application of EGTA and BAPTA is now the time course of

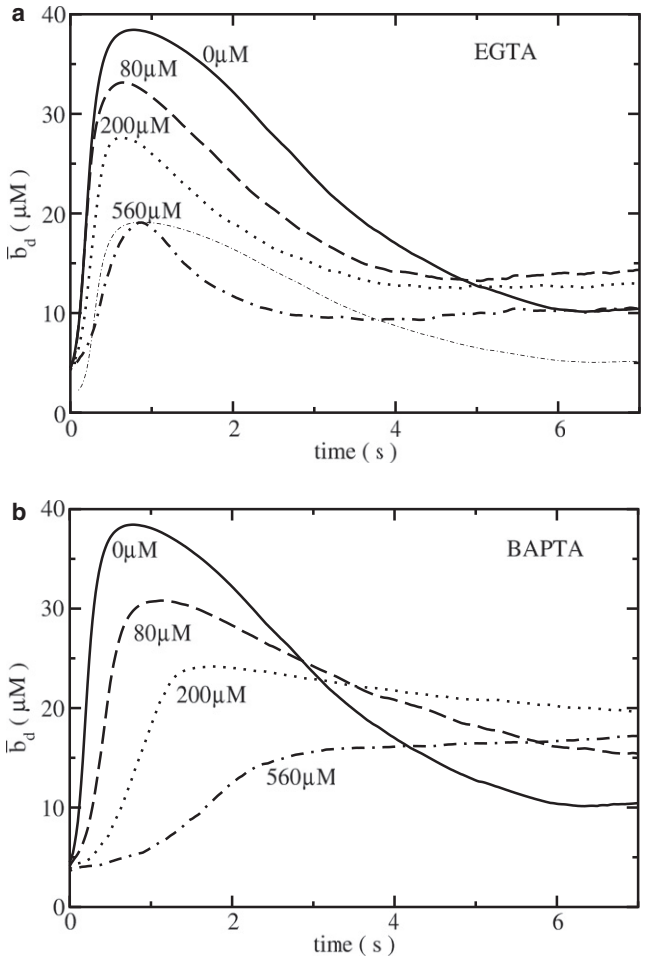

FIGURE 6 Evolution of bulk average of the concentration of Ca^{2+}-bound dye with small buffer diffusion $D_m = D_b = 20\ \mu m^2\ s^{-1}$ (averages of 10 runs each). The value of P_c was 36,000 s^{-1} in these simulations. The dash-dotted line in the EGTA panel is control rescaled to provide a direct illustration of the increased decay rate of $\bar{b}_d$ with large EGTA concentration.

the number of open channels. Its initial rise is much slower with BAPTA than with EGTA, and the maximum numbers reached with large BAPTA concentrations are much smaller than the control situation. Mutual activation of clusters is obviously reduced by large BAPTA concentrations. Again the number of open channels in the tail region is larger with BAPTA than with EGTA (see Fig. S6), but smaller than in the simulations with large buffer diffusion. Reducing D_m to 100 $\mu m^2\ s^{-1}$ only (instead of 20 $\mu m^2\ s^{-1}$) was sufficient to find the time course of the number of open channels in simulations with a larger cluster distance of 4.5 μm. We conclude that a large concentration of BAPTA with a small diffusion coefficient reduces spatial coupling between clusters, and thus abolishes mutual activation by Ca^{2+}. Clusters open asynchronously and some with very long delay. That causes the larger number of open channels in the tail region. The system goes to a stationary state with uncoordinated puffs.

Large concentrations of slowly diffusing buffer substantially slow down signal rise as Fig. 6 shows. That sets the time course of b_d with small buffer diffusion coefficient apart from the case with large buffer diffusion coefficient (compare Fig. 2).

CONCLUSIONS

We simulated the effect of exogenous buffer on the time course of Ca^{2+}-bound dye (and therefore fluorescence). Our simulation results agree well with the experimental findings (17,18). We extend the insights obtained from experiments by identifying buffer competition as an important contributor to the decay of Ca^{2+}-bound dye with EGTA as exogenous buffer, and by identifying delayed inhibition and decoupling and desynchronization as complementary mechanisms of release prolongation by BAPTA.

BAPTA shapes the time course of the number of open channels by reducing inhibition (if the buffer diffusion coefficient is large), or by decoupling clusters (when the diffusion coefficient is small). Simulations with large buffer diffusion appear more similar to the experiments by Dargan et al. (17) and Dargan and Parker (18) than those with small buffer diffusion, since the fluorescence signal with BAPTA is more in agreement with measured profiles. Hence, we believe that this is the mechanism applying to the experiments in *Xenopus* oocytes. However, changes in temperature or concentrations can change the viscosity of the cytosol, or other cell types may simply have a more viscous cytosol and therefore smaller diffusion coefficients. They may also have larger distances between clusters. That would entail weaker coupling by Ca^{2+}-diffusion and the desynchronization mechanism would apply.

Our model predicts that EGTA shortens fluorescence signals mostly by buffer competition and less by the shuttle effect. This prediction is based on the similarity of the time courses of line and bulk averages, and their weak dependence on the buffer diffusion coefficient. In the experiments of Dargan and Parker, the shuttle effect may contribute more to the shortening of the signal, by carrying Ca^{2+} ions away from the plane of clusters into the large bulk of the oocyte (18). However, we know from detailed three-dimensional simulations that steep gradients decay within tens of milliseconds (20). The timescales found in our study here and in experiments (see (18), their Fig. 6) correspond to profiles with small gradients which cannot drive large diffusional flux. Therefore, we do not expect the shuttle effect to become dominant. That implies that slow buffers could shape the fluorescence signal not only in large oocytes but in small cells also, which do not have a large space into which they can shuttle Ca^{2+}. That conclusion was very recently confirmed experimentally (33).

We see in Fig. S3 that the fluorescence signal does not report faithfully the time course of the number of open channels in control simulations. The shortening of the decay time of the fluorescence signal by EGTA entails that the signal follows the number of open channels more closely with large

[EGTA] than without it. That effect is exploited in recent experiments (33–35).

Here we investigate the first few seconds after onset of stimulation. Buffers also shape the asymptotic release dynamics reached after the initial transient. They may turn fast elevated sinusoidal oscillations into baseline spiking, as observed in hepatocytes and simulations (6,21). In mouse pancreatic acinar cells, EGTA and BAPTA both slow down the rise of global Ca^{2+} signals by decelerating the spread of release from the initiating release site across the secretory pole (36). That agrees with our findings here on the rise times of global signals. Large concentrations of EGTA decoupled the release sites in mouse pancreatic acinar cells. This resulted in desynchronization and an increase in global frequency due to independent spiking of subdomains of the secretory pole (36). These findings are very similar to the decoupling of release sites by EGTA found in SH-SY5Y cells (33). Large BAPTA concentrations appeared also to weaken spatial coupling between release sites since they slowed down the global signal rise. However, they did not lead to independently spiking subdomains. Instead, they allowed for a larger global signal than comparable EGTA concentrations, with the signal comprising the whole secretory pole, and spikes lasting longer (36). That is compatible with delayed inhibition as we observed in our simulations. The spikes with large BAPTA concentration are less frequent than control spikes and more random (21,36). The standard deviation of the interspike interval (ISI) is an indicator of spike probability (24). We conclude that a large concentration of BAPTA substantially reduces spike probability.

Recently published experimental results and earlier theoretical predictions analyze the behavior of repetitively spiking cells in detail (23–25). The spike frequency responds very sensitively to changes in the concentration of exogenous buffer in several cell types (24,25). Both EGTA and BAPTA increase the average ISI, and substantially increase the standard deviation. In other words, both EGTA and BAPTA reduce the spike probability (23,24). This can be reliably reproduced in simulations with cluster spacings larger than the 3 μm used here (23) and also with smaller distances in three dimensions (37). The simulations explain the increase of ISI and their standard deviation by a reduction of the strength of spatial coupling by buffers and the probability that a puff excites neighboring clusters (23,38). This was confirmed experimentally (24). EGTA required larger loading concentrations than BAPTA to obtain similar effects (25). Reduction of spike probability occurred at small exogenous buffer concentrations and larger concentrations abolished repetitive spiking (24). The reduction of the propensity for global events by EGTA and their suppression by BAPTA at low $[IP_3]$ found in this study (see Fig. 1 *a*) correspond to the increase of ISI and termination of repetitive spiking by EGTA and BAPTA, respectively.

The picture emerges that the action of buffers at low cluster density is different from the action at high cluster density. Since the strength of coupling by diffusion depends on cluster spacing and diffusion coefficients, the low cluster density case may be caused by small diffusion of free Ca^{2+} due to crowding (39), high viscosity, or high SR/ER Ca^{2+}-ATPase density (40). Low stimulation, such that not every cluster contains an activatable channel, also entails a low density situation.

At low cluster density, small concentrations of buffers applied to repetitively spiking cells increase the average ISI. Slow buffers applied to these cells act similarly to fast buffers, but require larger concentrations to have comparable effects on the ISI. Large buffer concentrations of either EGTA or BAPTA abolish oscillations by decoupling clusters (23,24,33,36). EGTA renders individual puffs distinguishable by increasing the gradients of fluorescence (called ''balkanization'').

Higher cluster densities require higher buffer concentrations to observe an effect in the first place. In contrast to the low density case, high buffer concentrations do not necessarily abolish repetitive spiking, as simulations (21,23) and experiments (36) showed. Slow buffers with large diffusion coefficient did not abolish spikes even at concentrations of 800 μM in our simulations here, whereas fast buffers with large diffusion coefficients abolish fluorescence spikes but not spikes in the number of open channels. Fast buffers with small diffusion coefficients can abolish these spikes also. The high cluster density regime exhibits a weak dependence of the rise time of the fluorescence signal on the BAPTA concentration in contrast to the low cluster density regime.

The repetitive spiking with high BAPTA concentrations observed by Kidd et al. (36) is not a contradiction to the results of this study, since it is a property of long time behavior that we did not investigate here. However, another question remains from a comparison of our results with those of Kidd et al. (36). Our results indicate that, when the BAPTA concentration is high and the stimulation level is high, the cell goes to a stationary state with a large fraction of inhibited channels. How is random spiking possible at all in this state? Is it random de-inhibition (which in theory can cause wave nucleation (41))? Further studies are required here.

Our simulations also provide for a more detailed understanding of balkanization of IP_3-mediated Ca^{2+} signals by EGTA (17,18). Balkanization means the disintegration of release patterns into isolated puffs by EGTA at IP_3 concentrations, which would cause waves without EGTA. We found balkanization with both large and small buffer diffusion coefficients. EGTA reduces, but does not eliminate, correlation between puff sites with the cluster distance used here (data not shown). BAPTA also reduces correlations between puff sites, and to a greater extent than EGTA. The reduction of coupling strength is due to the steepening of gradients of free Ca^{2+} by both EGTA and BAPTA and is one contribution to balkanization. Fluorescence profiles with comparable numbers of open channels in the tail region (see Figs. 1 and 4)

are spatially homogeneous with BAPTA but exhibit clearly distinguishable puffs with EGTA. EGTA increases the contrast between the bulk fluorescence (a short distance away from the clusters) and the fluorescence from open clusters, steepening spatial gradients of fluorescence as it increases temporal gradients. In contrast, BAPTA smears out fluorescence, so that despite the reduction of intercluster correlation, it is not an effective experimental tool to balkanize signals so as to study puffs in isolation.

Different cells express differing endogenous mobile Ca^{2+}-binding proteins with differing kinetics. For example, parvalbumin acts as a slow buffer and is in that sense similar to EGTA, whereas calretinin is a fast buffer with kinetics similar to BAPTA. Thus, cells could use buffers to control the properties of single spikes, as described here and found in experiments (17). What could they achieve by that? As Fig. S4 *a* shows, both buffers can control free cytosolic Ca^{2+} tightly with a concentration of 200 μM already. However, BAPTA does not allow for global spikes at that concentration, whereas EGTA still does. Thus, calretinin might be used to keep spatially averaged free cytosolic [Ca^{2+}] close to resting level and suppress spikes but not stationary release. Similar to EGTA, parvalbumin would also keep free cytosolic [Ca^{2+}] close to resting level in between spikes, and would still allow for spiking but with brief phases of high [Ca^{2+}]. Free [Ca^{2+}] would tightly follow the number of open channels with large parvalbumin concentrations.

SUPPORTING MATERIAL

Six figures and two tables are available at http://www.biophysj.org/biophysj/supplemental/S0006-3495(09)01103-5.

This work was supported by grant No. FA 350/6-1 of the Deutsche Forschungsgemeinschaft within the priority program SPP 1095 ''Analysis, Modeling, and Simulation of Multiscale Problems'', by the Marsden Fund of the Royal Society of New Zealand, and by the National Institutes of Health (USA) grant No. R01 DE016999-01.

REFERENCES

1. Parker, I., J. Choi, and Y. Yao. 1996. Elementary events of $InsP_3$-induced Ca^{2+} liberation in *Xenopus* oocytes: hot spots, puffs and blips. *Cell Calcium.* 20:105–121.
2. Lechleiter, J., S. Girard, E. Peralta, and D. Clapham. 1991. Spiral calcium wave propagation and annihilation in *Xenopus laevis* oocytes. *Science.* 252:123–126.
3. Marchant, J., and I. Parker. 2001. Role of elementary Ca^{2+} puffs in generating repetitive Ca^{2+} oscillations. *EMBO J.* 20:65–76.
4. Falcke, M. 2004. Reading the patterns in living cells—the physics of Ca^{2+} signaling. *Adv. Phys.* 53:255–440.
5. Berridge, M. 1990. Calcium oscillations. *J. Biol. Chem.* 265:9583–9586.
6. Rooney, T., E. Sass, and A. Thomas. 1989. Characterization of cytosolic calcium oscillations induced by phenylephrine and vasopressin in single Fura-2-loaded hepatocytes. *J. Biol. Chem.* 264:17131–17141.
7. Bezprozvanny, I., J. Watras, and B. Ehrlich. 1991. Bell-shaped calcium-response curves of $Ins(1,4,5)P_3$- and calcium-gated channels from endoplasmatic reticulum of cerebellum. *Nature.* 351:751–754.
8. Taylor, C., and A. Laude. 2002. IP_3 receptors and their regulation by calmodulin and cytosolic Ca^{2+}. *Cell Calcium.* 32:321–334.
9. Thomas, D., P. Lipp, M. Berridge, and M. Bootman. 1998. Hormone-evoked elementary Ca^{2+} signals are not stereotypic, but reflect activation of different size channel clusters and variable recruitment of channels within a cluster. *J. Biol. Chem.* 273:27130–27136.
10. Suhara, W., M. Kobayashi, H. Sagara, K. Hamadad, T. Goto, et al. 2006. Visualization of inositol 1,4,5-trisphosphate receptor by atomic force microscopy. *Neurosci. Lett.* 391:102–107.
11. Marchant, J., N. Callamaras, and I. Parker. 1999. Initiation of IP_3-mediated Ca^{2+} waves in *Xenopus* oocytes. *EMBO J.* 18:5285–5299.
12. Berridge, M., P. Lipp, and M. Bootman. 2000. The versatility and universality of calcium signaling. *Nat. Rev. Mol. Cell Biol.* 1:11–22.
13. Rooney, T., S. Joseph, C. Queen, and A. Thomas. 1996. Cyclic GMP induces oscillatory calcium signals in rat hepatocytes. *J. Biol. Chem.* 271:19817–19825.
14. Adkins, C., and C. Taylor. 1999. Lateral inhibition of Inositol 1,4,5-trisphosphate receptors by cytosolic Ca^{2+}. *Curr. Biol.* 9:1115–1118.
15. Mak, D.-O. D., J. E. Pearson, K. P. C. Loong, S. Datta, M. Fernández-Mongil, et al. 2007. Rapid ligand-regulated gating kinetics of single inositol 1,4,5-trisphosphate receptor Ca^{2+} release channels. *EMBO Rep.* 8:1044–1051.
16. John, L. M., M. Mosquera-Caro, P. Camacho, and J. D. Lechleiter. 2001. Control of IP_3-mediatedCa^{2+} puffs in *Xenopus laevis* oocytes by the Ca^{2+}-binding protein parvalbumin. *J. Physiol.* 535:3–16.
17. Dargan, S. L., B. Schwaller, and I. Parker. 2004. Spatiotemporal patterning of IP_3-mediated Ca^{2+} signals in *Xenopus* oocytes by Ca^{2+}-binding proteins. *J. Physiol.* 556:447–461.
18. Dargan, S., and I. Parker. 2003. Buffer kinetics shape the spatiotemporal patterns of IP_3-evoked Ca^{2+} signals. *J. Physiol.* 553:775–788.
19. Wagner, J., and J. Keizer. 1994. Effects of rapid buffers on Ca^{2+} oscillations and Ca^{2+} diffusion. *Biophys. J.* 67:447–456.
20. Thul, R., and M. Falcke. 2004. Release currents of IP_3 receptor channel clusters and concentration profiles. *Biophys. J.* 86:2660–2673.
21. Falcke, M. 2003. Buffers and oscillations in intracellular Ca^{2+} dynamics. *Biophys. J.* 84:28–41.
22. Bentele, K., and M. Falcke. 2007. Quasi-steady approximation for ion channel currents. *Biophys. J.* 93:2597–2608.
23. Falcke, M. 2003. On the role of stochastic channel behavior in intracellular Ca^{2+} dynamics. *Biophys. J.* 84:42–56.
24. Skupin, A., H. Kettenmann, U. Winkler, M. Wartenberg, H. Sauer, et al. 2008. How does intracellular Ca^{2+} oscillate: by chance or by the clock? *Biophys. J.* 94:2404–2411.
25. Skupin, A., and M. Falcke. 2007. Statistical properties and information content of calcium oscillations. *Genome Informatics.* 18:44–53.
26. DeYoung, G., and J. Keizer. 1992. A single-pool inositol 1,4,5-trisphosphate-receptor-based model for agonist-stimulated oscillations in Ca^{2+} concentration. *Proc. Natl. Acad. Sci. USA.* 89:9895–9899.
27. Thomas, R. C., and M. Postma. 2007. Dynamic and static calcium gradients inside large snail (*Helix aspersa*) neurones detected with calcium-sensitive microelectrodes. *Cell Calcium.* 41:365–378.
28. Adler, E. M., G. J. Augustine, S. N. Duffy, and M. P. Charlton. 1991. Alien intracellular calcium chelators attenuate neurotransmitter release at the squid giant synapse. *J. Neurosci.* 11:1496–1507.
29. Timmerman, M., and C. Ashley. 1986. FURA-diffusion and its use as an indicator of transient free calcium changes in single striated muscle cells. *FEBS.* 209:1–8.
30. Klingauf, J., and E. Neher. 1997. Modeling buffered Ca^{2+} diffusion near the membrane: implications for secretion in neuroendocrine cells. *Biophys. J.* 72:674–690.

31. Schmidt, H., E. B. Brown, B. Schwaller, and J. Eilers. 2003. Diffusional mobility of parvalbumin in spiny dendrites of cerebellar Purkinje neurons quantified by fluorescence recovery after photobleaching. *Biophys. J.* 84:2599–2608.

32. Schmidt, H., O. Arendt, E. B. Brown, B. Schwaller, and J. Eilers. 2007. Parvalbumin is freely mobile in axons, somata and nuclei of cerebellar Purkinje neurones. *J. Neurochem.* 100:727–735.

33. Smith, I. F., S. M. Wiltgen, and I. Parker. 2009. Localization of puff sites adjacent to the plasma membrane: functional and spatial characterization of Ca^{2+} signaling in SH-SY5Y cells utilizing membrane-permeant caged IP_3. *Cell Calcium.* 45:65–76.

34. Demuro, A., and I. Parker. 2008. Multi-dimensional resolution of elementary Ca^{2+} signals by simultaneous multi-focal imaging. *Cell Calcium.* 43:367–374.

35. Smith, I. F., and I. Parker. Imaging the quantal substructure of single IP3R channel activity during Ca^{2+} puffs in intact mammalian cells. *Proc. Natl. Acad. Sci.* 106:6404–6409.

36. Kidd, J. F., K. E. Fogarty, R. A. Tuft, and P. Thorn. 1999. The role of Ca^{2+} feedback in shaping $InsP_3$-evoked Ca^{2+} signals in mouse pancreatic acinar cells. *J. Physiol.* 520:187–201.

37. Rahman, T.-U., A. Skupin, M. Falcke, and C. W. Taylor. 2009. Clustering of IP_3 receptors by IP_3 retunes their regulation by IP_3 and Ca^{2+}. *Nature.* 458:655–659.

38. Falcke, M. 2007. Mechanism of intracellular Ca^{2+} oscillations and interspike interval distributions. *In* Noise and Fluctuations in Biological, Biophysical, and Biomedical Systems. S. M. Bezrukov, editor. *Proc. SPIE.* 6602:0M1-0M12.

39. Ölveczky, B., and A. Verkman. 1998. Monte Carlo analysis of obstructed diffusion in three dimensions: application to molecular diffusion in organelles. *Biophys. J.* 74:2722–2730.

40. Schipke, C. G., A. Heidemann, A. Skupin, O. Peters, M. Falcke, et al. 2008. Temperature and nitric oxide control spontaneous calcium transients in astrocytes. *Cell Calcium.* 43:285–295.

41. Henry, H., and H. Levine. 2003. Wave nucleation rate in excitable systems in the low noise limit. *Phys. Rev. E Stat. Nonlin. Soft Matter Phys.* 68:0131914.